

On the location and orientation of the South Pacific Convergence Zone

Matthew J. Widlansky · Peter J. Webster ·
Carlos D. Hoyos

Received: 8 June 2009 / Accepted: 18 June 2010
© Springer-Verlag 2010

Abstract Three semi-permanent cloud bands exist in the Southern Hemisphere extending southeastward from the equator, through the tropics, and into the subtropics. The most prominent of these features occurs in the South Pacific and is referred to as the South Pacific Convergence Zone (SPCZ). Similar bands, with less intensity, exist in the South Indian and Atlantic oceans. We attempt to explain the physical mechanisms that promote the diagonal orientation of the SPCZ and the processes that determine the timescales of its variability. It is argued that the slowly varying sea surface temperature patterns produce upper tropospheric wind fields that vary substantially in longitude. Regions where 200 hPa zonal winds decrease with longitude (i.e., negative zonal stretching deformation, or $\partial\bar{U}/\partial x < 0$) reduce the group speed of the eastward propagating synoptic (3–6 day period) Rossby waves and locally increase the wave energy density. Such a region of wave accumulation occurs in the vicinity of the SPCZ, thus providing a physical basis for the diagonal orientation and earlier observations that the zone acts as a “graveyard” of propagating synoptic disturbances. In essence, $\partial\bar{U}/\partial x = 0$ demarks the boundary of the graveyard while regions where $\partial\bar{U}/\partial x < 0$ denote the graveyard itself. Composites of the life cycles of synoptic waves confirm this hypothesis. From the graveyard hypothesis comes a more general theory accounting for the SPCZ’s spatial orientation and its longer term variability influenced by the El Niño–Southern Oscillation (ENSO), or alternatively, the changing background SST associated with different phases of ENSO.

Keywords Southern Hemisphere Convergence Zones · South Pacific Convergence Zone · Wave energy accumulation · Zonal stretching deformation · El Niño–Southern Oscillation

1 Introduction

An infrared view of Earth (Fig. 1) reveals a number of persistent climate features. Subtropical oceans coincide with outgoing longwave radiation (OLR) maxima, indicating emission to space from the ocean surface with little attenuation. Minima in OLR, usually associated with deep convection, are associated with equatorial continental regions (including the Indonesian archipelago), the tropical warm pools of the Pacific and Indian oceans, and baroclinic disturbances in the mid-latitudes. In the tropics, deep convection is collocated with the warmest sea surface temperatures (SSTs) except in regions of strong cross-equatorial pressure gradients in the lower troposphere where convection lies equatorward of the maximum SST (Toma and Webster 2009). There are also a number of equally prominent regions where deep convection (minimum OLR) appears to connect equatorial convective regions with baroclinic zones of the extratropical Southern Hemisphere. The most prominent of these bands is the South Pacific Convergence Zone (SPCZ) stretching between the warm pool convection and the South Pacific. Somewhat weaker are the South Indian Convergence Zone (SICZ) and the South Atlantic Convergence Zone (SACZ). There is little evidence of similar bands in the Northern Hemisphere.

Existence of persistent and organized convective regions in the Southern Hemisphere became apparent at the beginning of the satellite era. A number of studies

M. J. Widlansky (✉) · P. J. Webster · C. D. Hoyos
School of Earth and Atmospheric Sciences, Georgia Institute
of Technology, Atlanta, GA 30332, USA
e-mail: matthew.widlansky@eas.gatech.edu

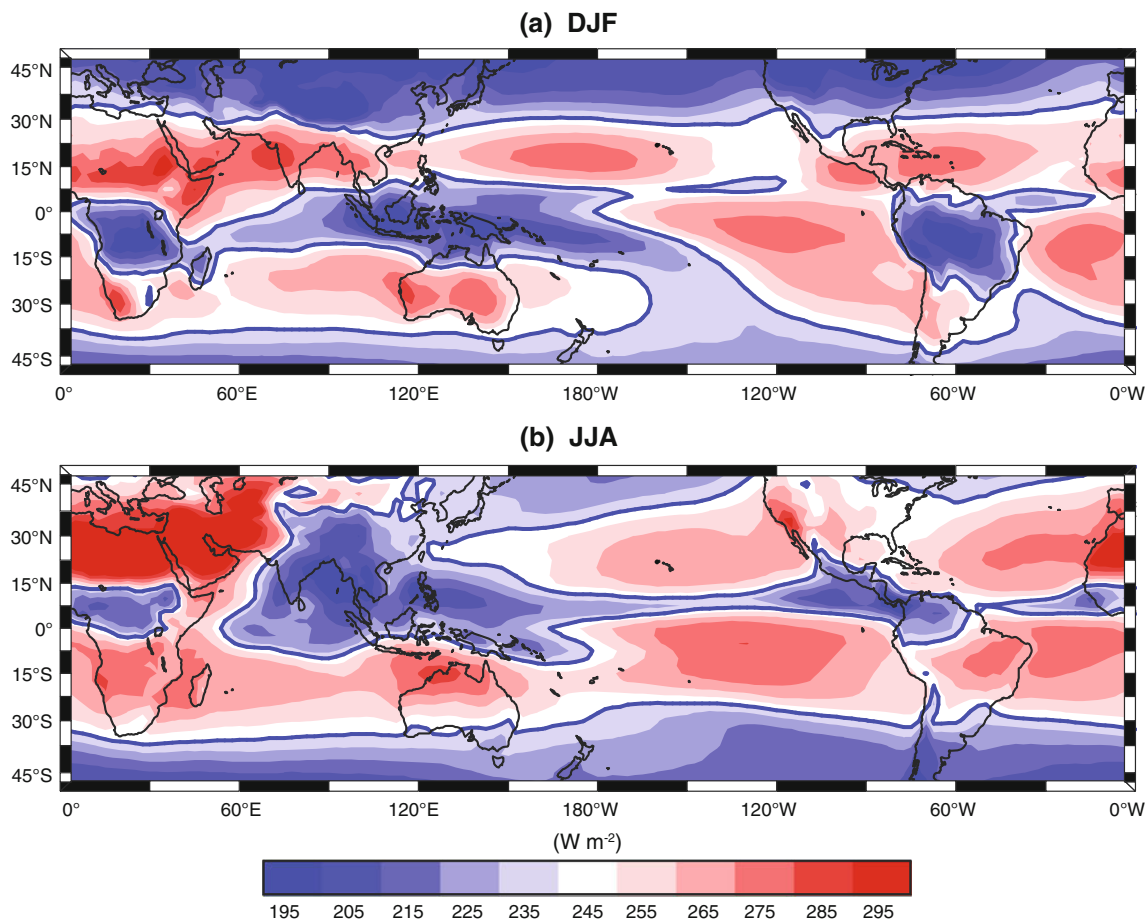


Fig. 1 Global climatology (1982–2008) of OLR (W m^{-2}) for **a** DJF and **b** JJA. 240 W m^{-2} OLR contour outlined by blue lines in each panel

(Kornfield et al. 1967; Godshall 1968; Bjerknes et al. 1969; Booth and Taylor 1969; Leese et al. 1970; Streten 1970; Taljaard 1972) noted predominant bright bands extending zonally and meridionally across the three Southern Hemisphere oceanic basins. These observations were consolidated by Streten (1973) who noted that the bands were regions of widespread convective activity and precipitation extending into the mid-latitudes from the equatorial land masses of Africa, the Indonesian archipelago, and the Amazon basin. Furthermore, Streten (1973) noted that the three bands were associated with long wave circulation patterns, described earlier by van Loon and Jenne (1972), and highly active on synoptic time scales. These features tended to be most stable in the South Pacific and South Atlantic but more variable in location and intensity, and with smaller magnitude, in the South Indian Ocean.

Overall, the majority of studies have concentrated on the most apparent and enduring of the convective bands: the SPCZ (e.g., Trenberth 1976; Vincent 1994; Karoly and Vincent 1999); finding within the extensive cloud band pronounced spatial and temporal differences between the

equator, tropics, and subtropics. Tropical convection, for example, is oriented zonally, associated with strong boundary layer convergence (e.g., Vincent 1994; Lintner and Neelin 2008), and located along gradients of SST (e.g., Lindzen and Nigam 1987). Further south, in the subtropics, the SPCZ becomes more diagonally oriented and appears to possess baroclinic-type disturbances with 4–5 day periodicities originating south of the Australian region (Streten 1973; Streten and Zillman 1984; Kiladis et al. 1989; Trenberth 1991). Streten (1973) found similar time scales of variability in the subtropical portions of the SACZ and SICZ as well. Variability in the tropical SPCZ, on the other hand, is dominated by periodicities longer than 2 weeks. The differences in variance periodicities with latitude suggest that the tropical and higher latitude SPCZ are influenced by different dynamical processes. However, the similar poleward slope of the three cloud bands suggests that the zones possess common roots.

Fewer studies have considered the SICZ and SACZ, although these were included in the satellite climatology of Kuhnel (1989). Like the SPCZ, the other bands show variability over a wide range of time scales. The location

and variability of the SICZ is critical with respect to the rainfall of southern Africa (van Heerden and Taljaard 1998; Todd and Washington 1998, 1999; Carvalho et al. 2002; Nicholson 2003). Similarly, Rickenbach et al. (2002) and Todd et al. (2003) find a dependency of South American rainfall on the variability of the SACZ. Linkages between variability in the Atlantic basin and the SPCZ are also observed (Rodwell and Hoskins 2001; Hoskins and Hodges 2005).

Interannual oscillations in the positioning of the SPCZ (Trenberth 1976, 1997; Streten and Zillman 1984; Karoly and Vincent 1999; Folland et al. 2002) suggest that slow SST modulations associated with the El Niño-Southern Oscillation (ENSO) may alter both the background climate circulation (e.g., Webster 1982; Juillet-Leclerc et al. 2006; Vincent et al. 2009) and the position of the diagonal cloud band. The quasi-stationary South Pacific SST pattern consists of large meridional and zonal temperature gradients. In the upper troposphere, winds are mostly easterly over the low latitude West Pacific warm pool and westerly in a concentrated jet stream to the south. Strong zonal gradients also exist in the wind field and appear spatially correlated with the underlying SST gradients. It is therefore reasonable to infer that the Pacific SST pattern may govern the positioning and intensity of not only basin-scale circulation features, but also the SPCZ. In essence, the location of the SPCZ is tied to the quasi-stationary long wave circulation of the hemisphere.

Many studies have proposed an important role for the East Pacific subtropical high in establishing a convective band to the west (e.g., Trenberth et al. 2000; Rodwell and Hoskins 2001; Trenberth and Stepaniak 2003; Takahashi and Battisti 2007b). Rodwell and Hoskins (2001), for example, describe how latent heating from monsoon convection over the Amazon basin strengthens the East Pacific high via an upstream Rossby wave response which produces adiabatic descent west of the Andes mountain range. Subsidence of low specific humidity air was later shown, through a series of modeling experiments (Takahashi and Battisti 2007a), to increase evaporative cooling in the East Pacific; thereby lowering the local SST. Takahashi and Battisti (2007b) suggest that the subtropical high enhances the SPCZ by acting as a blocking mechanism for eastward propagating mid-latitude cyclones and providing diffluent meridional flow in the upper troposphere as originally suggested by Trenberth et al. (2000). However, the actual physical mechanisms that constitute “blocking”, on one hand, and local intensification of convection and synoptic variance, on the other, remain obscure.

A clue to an overriding physical mechanism may be imbedded in the observations of Trenberth (1976). After describing the character of the SPCZ, he notes that the SPCZ “...tends to form a ‘graveyard’ region for fronts

moving from the southwest in the troughs of low pressure between the migratory anticyclones across Australia and New Zealand ...”. Trenberth (1991) also noted an association between the exit, or diffluent, region of the Southern Hemisphere subtropical jet stream and the location of the SPCZ. If the Trenberth (1976, 1991) observations are correct, then it would seem that the essence of an explanation may reside in the interactions of transient modes with the much more slowly varying background flow.

Other studies have suggested that the diagonal orientation of deep convection is related to the regional SST distribution as well as the location of the subtropical jet stream (Graham and Barnett 1987; Kiladis et al. 1989; Eastin and Vincent 1998; Yoshikane and Kimura 2003). Noting the importance of the SST distribution in forcing low-frequency atmospheric standing waves (e.g., van Loon and Jenne 1972; Webster 1982), these studies may be restating the notion that the SPCZ is forced by interactions between synoptic disturbances and low frequency variability of the background flow. Even so, there remains the basic question of why the quasi-stationary long waves produce regions of enhanced synoptic activity in three specific Southern Hemisphere locations.

Recently, the climate of the southwest Pacific has become a focal point of research initiatives based on the hypothesis that the SPCZ is closely coupled with regional oceanic circulations and associated with large-scale atmospheric teleconnections (Ganachaud et al. 2007). These concerns have led to the design of a regionally coordinated experiment, the CLIVAR Southwest Pacific Ocean Circulation and Climate Experiment (SPICE), aimed at understanding the role of ocean circulation in the large-scale, low-frequency modulation of climate and generation of local climate signatures, such as the SPCZ.

We focus on developing an understanding of why the SPCZ veers southward into higher latitudes away from the western Pacific Intertropical Convergence Zone (ITCZ). Furthermore, we explore why different periodicities dominate convective activity as a function of latitude. In the next section, we present a climatology of the SPCZ relative to both the long-term mean structure of the Southern Hemisphere and its higher frequency variance. In Sect. 3, we propose a hypothesis suggesting that slowly varying upper troposphere zonal winds, driven in part by strong zonal SST gradients, foster regions suitable for the modification of mid-latitude Rossby waves. Section 4 tests the hypothesis that mid-latitude disturbances amplify in the SPCZ region when the wave characteristics are modified by the low frequency variability of the basic background flow. The testing is accomplished by controlled experiments using an atmospheric general circulation model (AGCM) to examine the sensitivity of the zonal wind basic

state and SPCZ orientation to both the Pacific SST pattern and location of the continents. We also explore temporal correlations on interannual timescales between the Pacific zonal SST gradient and intensity of the SPCZ. Composites of synoptic disturbances propagating through the SPCZ are then used to measure wave characteristics and perform diagnostics of their vertical structure. Section 5 provides a summary of the results.

2 Climatology of the SPCZ

We examine in detail the 1982–2008 period within the region enclosed by 20°N–50°S and 120°E–70°W, defining the equatorial and southern parts of the Pacific basin. The DJF mean fields of OLR (Fig. 2a), following Liebmann and Smith (1996), show the SPCZ (enclosed by the 240 W m^{-2} OLR contour) extending from the tropical warm pool convection of the western Pacific in a

southeastward direction towards the Southern Hemisphere mid-latitudes. DJF is chosen as it encloses the period of the year when the deepest convection occurs in the SPCZ. A narrow equatorial strip of low OLR is associated with the relatively weak boreal winter Northern Hemisphere ITCZ. Stark longitudinal differences are apparent. In the western part of the region, two convective maxima, associated with deep convection over Indonesia and a zone of extratropical disturbances, are separated by a convective minimum over Australia. The northern maximum extends eastward across the tropical warm pool, slopes southeast, and joins the extratropical convective maximum through the diagonally oriented SPCZ. To the east of the SPCZ, OLR values increase substantially indicating minimum convection and subsidence over the Pacific subtropical high pressure system.

The OLR standard deviation over the Pacific basin exceeds 35–50 W m^{-2} along a diagonal band corresponding to the climatological orientation of the SPCZ.

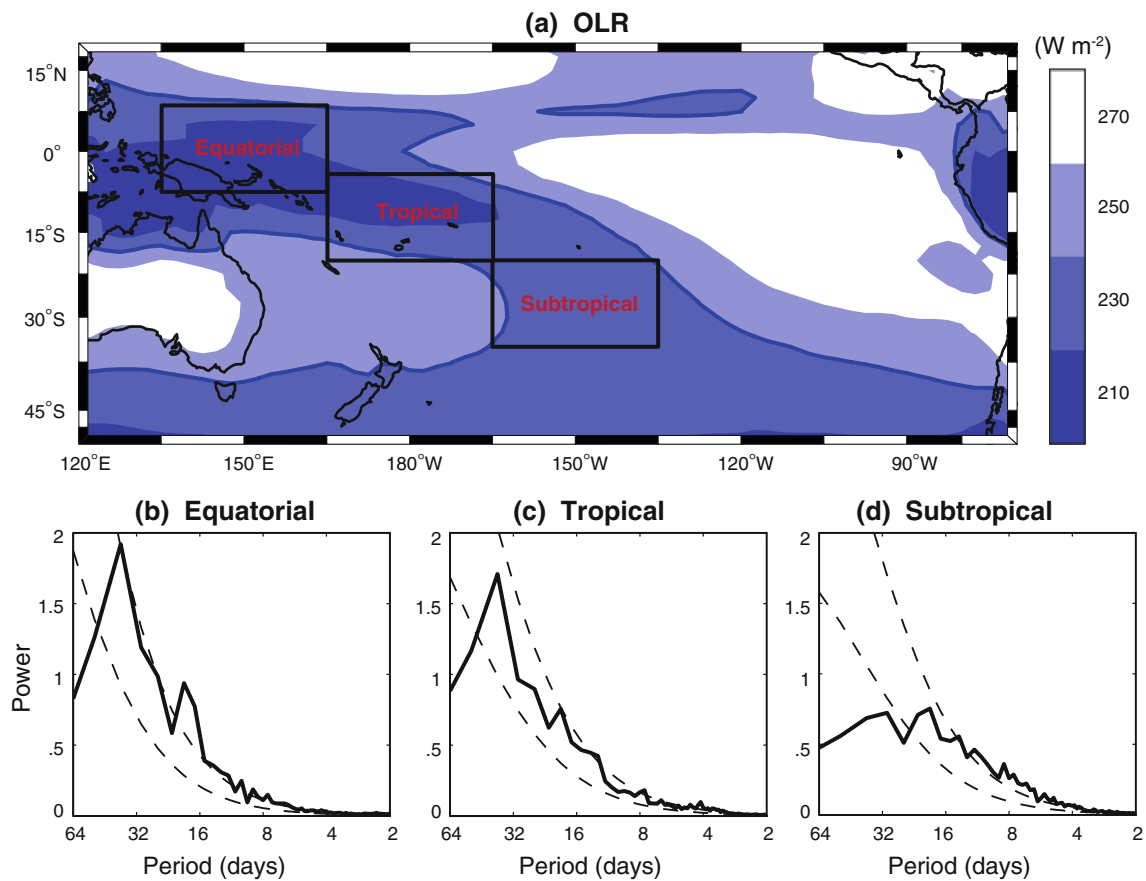


Fig. 2 a DJF climatology (1982–2008) of OLR (W m^{-2}). 240 W m^{-2} OLR contour outlined by blue lines. Black boxes represent the “Equatorial” (7.5°N–7.5°S, 135°E–165°E), “Tropical” (5°S–20°S, 165°E–165°W), and “Subtropical” (20°S–35°S, 165°W–135°W) averaging regions for calculating OLR time series. b, c, and d

Normalized Fourier power spectra of NDJFM (1982–2008) OLR in the equatorial, tropical, and subtropical regions of the SPCZ, respectively. Lower dashed lines are the red-noise spectra for mean lag-1 autocorrelations of 0.90 (b), 0.78 (c), and 0.70 (d). Upper dashed lines are the 95% confidence spectra

Normalized Fourier power spectra of OLR time series are used to compare the modes of variability for the equatorial, tropical, and subtropical SPCZ regions (Fig. 2b–d, respectively). Here, we use November through March (NDJFM) daily OLR anomalies to provide 27 seasonal time series of sufficient temporal resolution and length for analyzing synoptic (3–6 day) to intraseasonal (30–60 day) variability. Red-noise spectra (lower-dashed lines) for mean lag-1 autocorrelations of 0.90 (b), 0.78 (c), and 0.70 (d) along with the corresponding 95% confidence spectra (upper-dashed lines) are calculated using the methods of Torrence and Compo (1998) with the assumption that each season is independent. This provides 26 degrees of freedom.

In the equatorial and tropical SPCZ, variability peaks around 2 weeks and between 30 and 60 days (Fig. 2b and c, respectively) with variance decreasing markedly towards shorter time scales. These spectra suggest that equatorward of 20°S, the SPCZ is strongly influenced by intraseasonal variability (e.g., the Madden-Julian oscillation) and other convective oscillations on timescales greater than 2 weeks. While some evidence of a 2 week spectral peak also exists in the subtropical time series (Fig. 2d), most of the significant OLR variability is constrained to synoptic timescales of less than 8 days. Mean lag-1 autocorrelations also decrease away from the tropics. The shift toward higher frequency variability poleward of 20°S suggests that synoptic disturbances provide most of the convective variance in the subtropical part of the SPCZ.

Figure 3a–d displays, respectively, the 200 hPa geopotential height and wind from the NCEP–NCAR reanalysis data (Kalnay et al. 1996; Kistler et al. 2001), the 200 hPa zonal wind component (\bar{U}), the SST from Reynolds et al. (2002), and the large-scale zonal SST gradient during DJF. In all four panels, the bold blue contour (OLR = 240 W m⁻² from Fig. 2a) encloses the deep penetrative convection across the SPCZ and outlines clearly the poleward extent of the diagonal convective zone. The large black box (labeled “A” in Fig. 3c) extends from 20°S to 35°S and denotes the subtropical region where time series of OLR and dynamical quantities will be extracted. The two smaller boxes (“B” and “C” in Fig. 3c) are used to compute zonal gradients of SST. Superimposed on the upper tropospheric zonal wind field and zonal SST gradient (Fig. 3b and d, respectively) are contours of $\partial\bar{U}/\partial x < 0$, the negative stretching deformation of the zonal wind field.

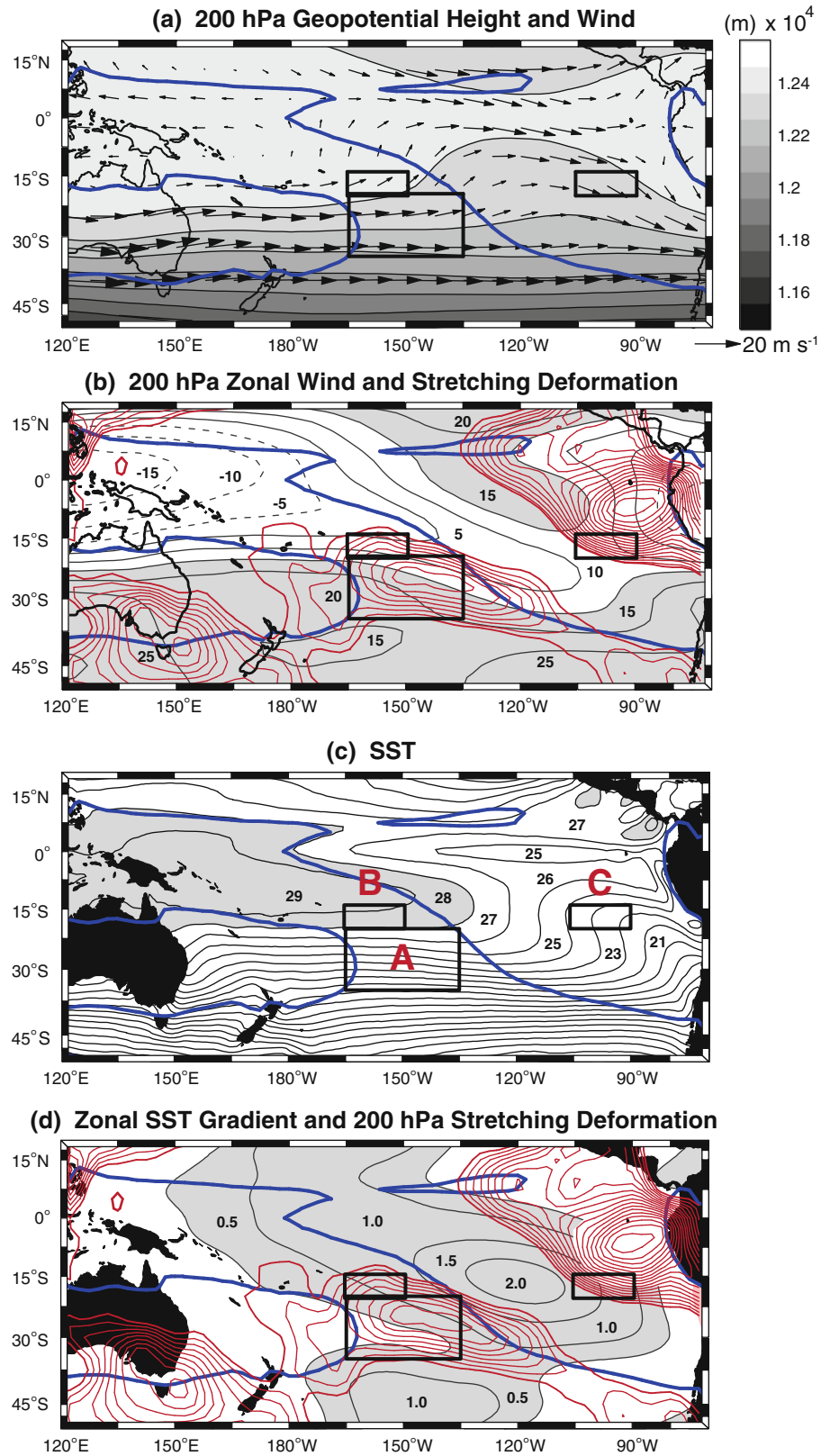
Figure 3a shows the upper tropospheric geopotential height and wind field. The analysis is performed at the 200 hPa level to determine steering currents of mid-latitude synoptic waves which may impact the SPCZ diagonal region. In general, the height of the 200 hPa wind field

parallels the SST distribution with greater heights occurring over warm SSTs and lower heights over cooler regions. Meridional height gradients are enhanced over the western and eastern parts of the Pacific basin and consistent with the location of the subtropical jet stream maxima near Australia and South America. Westerly winds (Fig. 3b) greater than 15 m s⁻² are shaded to highlight the subtropical jet stream location (poleward of 20°S), as well as equatorial westerlies over the central Pacific. To the northeast of the SPCZ, strong westerlies extend from the Northern Hemisphere into the central South Pacific. This is the “westerly duct” (Webster and Holton 1982; Tomas and Webster 1994; Duane et al. 1999) through which disturbances of one hemisphere can potentially influence the other hemisphere over a wide range of frequencies. The diagonal SPCZ (enclosed by the blue contours between 20°S and 35°S) lies in a region of decreasing westerly winds to the east of the Australian subtropical jet stream maximum (i.e., the jet stream exit region). Negative zonal stretching deformation ($\partial\bar{U}/\partial x < 0$) is depicted by red contours. For later reference, these contours show maximum values in the exit region of the subtropical jet stream denoted by box A. At this stage, we note that a region of negative zonal stretching deformation is collocated with the SPCZ in the subtropics.

The corresponding SST climatology (Reynolds et al. 2002) is shown in Fig. 3c. Temperatures greater than 28°C are shaded to designate the spatial extent of the West Pacific warm pool. A basin-scale meridional (zonal) SST gradient is observed south (southeast) of the warm pool. The eastern boundary of the SPCZ (defined arbitrarily by the 240 W m⁻² OLR contour between 20°S and 35°S) transects the meridional SST gradient and is located southwest of the maximum zonal SST gradient, which exceeds 5°C across the subtropical South Pacific. This gradient is calculated as the difference between the mean SST in box B and box C which are separated by about 6,300 km.

Figure 3d shows the zonal component of the SST gradient calculated following the methods of Rowell (2001). Two SST averaging boxes (15° latitude by 60° longitude) are defined for each grid point such that the latitudes of their centers are the same latitude as the grid point. The relative dimensions of the averaging boxes reflect the greater length-scale of SST anomalies in the zonal direction and approximate the longitudinal distance between boxes B and C. Each grid point separates a “western” and “eastern” box. The difference between their average SSTs, divided by the distance between their centers, is the large-scale zonal SST gradient (°C 1,000 km⁻¹). Gray shading indicates where SSTs decrease from west to east; on condition that at least 40% of each averaging box is open water. Minimum OLR and regional $\partial\bar{U}/\partial x < 0$ are

Fig. 3 DJF climatology (1982–2008) of **a** 200 hPa geopotential height (m, *shading*) and wind (*vectors*). **b** 200 hPa zonal wind (5 m s^{-1} interval, *dashed lines* depict negative zonal wind, zero contour omitted, *gray shading* indicates zonal wind greater than 15 m s^{-1}) and zonal stretching deformation (s^{-1} , *red contours*). Zonal stretching deformation contour interval: $-5 \times 10^{-7} \text{ s}^{-1}$; *thick lines* depict the zero contour. **c** SST (1°C interval, *gray shading* indicates temperatures above 28°C). **d** Zonal SST gradient ($^\circ\text{C } 1,000 \text{ km}^{-1}$, *shading*) and 200 hPa zonal stretching deformation (s^{-1} , *red contours*). *Large black box* (“A” located at 20°S – 35°S , 165°W – 135°W) represents the averaging region for calculating OLR and stretching deformation time series. *Small black boxes* (“B” and “C” located at 14.5°S – 20.5°S , 165.5°W – 149.5°W and 14.5°S – 20.5°S , 105.5°W – 89.5°W , respectively) denote regions used to calculate the SST index. 240 W m^{-2} OLR contour outlined by *blue lines* in each panel



collocated in the subtropical SPCZ (box A) and positioned slightly poleward of the maximum large-scale zonal SST gradient (confirmed by Fig. 3d to be between box B and

box C). Statistical relationships between SST, OLR, and the character of the zonal mean flow are described further in Sect. 4.2.

3 Hypothesis

Figure 3b shows that there is a complex latitudinal and longitudinal structure to the observed zonal wind field. Zhang and Webster (1989) explored the dynamical impacts of the sign of the basic zonal flow and the degree of latitudinal shear in zonally symmetric atmospheres. Relatively small differences were found in wave structure and propagation speed for easterly or westerly equatorial winds. But a comparison of Figs. 2a and 3b suggests less subtle relationships between longitudinal variations of convection and the basic state; especially between low OLR and $\partial\bar{U}/\partial x < 0$ in the diagonal portion of the SPCZ such as in box A. For later reference, note that the negative stretching deformation region exists southwest of a large SST zonal gradient between boxes B and C, as shown in Fig. 3d.

The relationship between longitudinal stretching deformation of the climatological background state and imbedded transients has been studied extensively although principally with a low-latitude focus, such as in the lower troposphere of the tropical SPCZ. Numerical experiments with a wave source in a longitudinally varying basic flow (Webster and Holton 1982) showed evidence of transients being trapped in regions where $\partial\bar{U}/\partial x < 0$. To first approximation, such trapping, together with the increase in regional wave energy density, occurs when the longitudinal group speed of the mode (C_{gx}) approaches zero. But a series of studies (Webster and Chang 1988, 1997; Chang and Webster 1990, 1995) showed that there are also kinematic implications of waves propagating through a zonally varying basic flow. Based on earlier work of Bretherton and Garrett (1968) and Lighthill (1978), a series of rules were derived relating the structure and energy of waves to the character of the background zonal flow. Under the constraints that the background wind field varies gradually in space and the frequency of synoptic-scale Rossby waves is conserved, Webster and Chang (1997) derived the following expressions:

$$\frac{dk}{dt} = -k \frac{\partial\bar{U}}{\partial x} \tag{1}$$

$$\frac{d\xi}{dt} = -\xi \frac{\partial\bar{U}}{\partial x} \tag{2}$$

Here, k is the longitudinal wave number emerging from the assumption of normal mode solutions of the form $\propto i(kx + mz - \omega_r t)$, where m is the vertical wave number and ω_r is the intrinsic frequency of the mode in a frame of reference where $\bar{U} = 0$ (Webster and Chang 1988). ξ is the wave energy density given by $\xi = \rho gh^2/2$, where ρ is density and h is the equivalent depth of the mode. The wave action density (ε), conserved along a ray (i.e., along a

path defined as $dx/dt = C_{gd}$), is essentially ξ divided by ω_r (Lighthill 1978). The substantial derivative is defined to follow the local group velocity of the mode, $C_{gd} = \bar{U}(x) + C_{gx}$, and is given by:

$$\frac{d}{dt} = \frac{\partial}{\partial t} + C_{gd} \frac{\partial}{\partial x} \tag{3}$$

The Doppler-shifted group speed is defined as:

$$C_{gx} = - \left[\frac{\beta(k^2 + \beta(2n + 1)/c) - 2k^2\beta}{(k^2 + \beta(2n + 1)/c)^2} \right] \tag{4}$$

on an equatorial β -plane, where $c = \sqrt{gh}$ and n is the latitudinal nodal number. Details of Rossby wave propagation in a heterogeneous zonal flow are given in Webster and Chang (1997) and only the salient properties are presented here. These are:

- (i) The group velocity for synoptic-scale Rossby waves is eastward relative to the basic state.
- (ii) Changes in the scale of the wave are determined by the sign of the zonal stretching deformation. From (1), if $\partial\bar{U}/\partial x < 0$ then k will increase along a ray, hence decreasing its longitudinal scale. As k increases, the longitudinal group speed C_{gx} will correspondingly decrease, as can be seen from (4).
- (iii) From (2), if $\partial\bar{U}/\partial x < 0$ then the wave energy density will increase along a ray.

We pose the hypothesis that eastward propagating mid-latitude disturbances encounter a region of negative zonal stretching deformation in the upper troposphere where their longitudinal extent shrinks, their group speed is reduced, and wave energy “accumulates” (i.e., locally increases). The expected result is a highly energetic convective region (i.e., low OLR) oriented diagonally away from the equator in the South Pacific.

4 Testing the hypothesis

To test the hypothesis, we need to determine the factors that control the Southern Hemisphere circulation patterns which produce a region of negative zonal stretching deformation in the region of the SPCZ. Furthermore, we need to provide evidence that disturbances passing through such a region are modified according to (1) and (2). We use controlled numerical experiments with a global climate model to address the first problem and then quantify interannual changes in the observed SPCZ. The second problem is addressed by compositing synoptic disturbances as they enter the negative zonal stretching deformation region. We compute **Q** vectors to analyze the modification of these disturbances.

4.1 Longitudinal variability of the climatological circulation

To gain an understanding of the factors that determine the background basic state of the Southern Hemisphere, we conduct a series of controlled numerical experiments using the International Centre for Theoretical Physics (ICTP) AGCM (Molteni 2003; Bracco et al. 2004; Kucharski et al. 2006, 2009). Kucharski et al. (2009) describe the AGCM as based on a hydrostatic spectral dynamical core (Held and Suarez 1994) and governed by many parameterized processes including short- and long-wave radiation, large-scale condensation, convection, surface fluxes of momentum, heat and moisture, and vertical diffusion. The idealized AGCM is configured with eight vertical (sigma) levels and with a spectral truncation at total wavenumber 30. In all experiments, the model is initialized from an atmosphere at rest and integrated for a 26 year period. The first 2 years of integration are discarded and the 24 remaining years used to compile DJF seasonal averages.

Three experiments are conducted:

- (i) A “Control” run, where the model is forced by a fixed annual cycle of monthly climatological SSTs and land boundary conditions. Data are from the European Centre for Medium-Range Weather Forecasts’ re-analysis (ERA15: Gibson et al. 1997) and averaged over the 1981–1990 period to achieve a balance between warm and cold ENSO events in the SST field. The Control experiment describes the model response to a prescribed annual cycle of SST.
- (ii) An “SST” experiment configured to test the importance of the zonal gradient of Pacific SST in forcing the quasi-stationary characteristics of the Southern Hemisphere. Specifically, the SST distribution of the Control experiment in the Pacific basin (61°N–61°S, 121°E–112°W) is replaced with the zonal average of the observed values by setting $dSST_{Pacific}/dx = 0$. The zonally averaged SST maintains an annual cycle consistent with the monthly varying climatology. Elsewhere, SSTs have the same evolving climatological annual cycle used in the Control experiment. Large changes to the SST field are mostly confined to the tropics and subtropics because the observed zonal SST gradient used in the Control experiment is small poleward of 35°S, especially during DJF.
- (iii) An “Orography” experiment examines the circulation response to the removal of orography in a channel between 61°N and 61°S. In this zonal aqua-channel experiment, land surfaces are treated as ocean in the model by using observed land surface temperatures to prescribe an artificial SST pattern. Land albedo is also lowered to match an ocean

surface. Elsewhere, climatological boundary sea and land conditions are used. In essence, we attempt to determine the role of orography in forcing the DJF climatology.

The purpose of the experiments is not to simulate exactly the observed atmospheric structure of the Southern Hemisphere. Such a task would have to be performed using a much higher resolution model. Rather, we attempt to determine the changes in simulated climatologies relative to the Control with, or without, SST alterations and orographic forcing factors.

Figure 4 shows the Southern Hemisphere DJF climatology of simulated OLR and 200 hPa zonal wind (left and right columns, respectively) for the (a) Control, (b) SST, and (c) Orography experiments. Departures from the Control simulation are shown for the SST and Orography experiments. Comparison of Fig. 4a (left column) with observed OLR (Fig. 2a) indicates that the AGCM simulates a diagonal band of convection similar in location and intensity to the observed SPCZ, although the modeled convective zone is more zonally oriented. Lin (2007) also finds a zonal bias of the SPCZ in an analysis of 22 coupled GCMs; however, complex coupled models often depict a South Pacific cloud band oriented almost parallel to the ITCZ. The idealized AGCM simulates a 200 hPa westerly wind maximum between 30°S and 50°S and easterlies over the West Pacific warm pool (Fig. 4a, right column) but with some biases. The Control climatology possesses a westerly duct in the eastern equatorial Pacific, although it is weaker than observed. There is also an equatorward shift of the Southern Hemisphere jet stream, resulting in a positive \bar{U} bias exceeding 10 m s^{-1} throughout the diagonal SPCZ region at 20°S–35°S. Molteni (2003) documented similar 200 hPa zonal wind biases in simulations of the Southern Hemisphere.

Figure 5 shows the simulated OLR (blue) and 200 hPa zonal stretching deformation (red), averaged between 20°S and 35°S, across the Pacific basin for each of the three experiments. Gray shading represents regions of $\partial\bar{U}/\partial x < 0$ for the Control experiment (solid lines). In general, the Control shows a reasonable coincidence between low OLR and regions of $\partial\bar{U}/\partial x < 0$. A notable difference is evident between 150°W and 130°W where convection is simulated but with a positive or near-zero zonal stretching deformation for each experiment.

Removal of the Pacific zonal SST gradient (SST experiment) produces strong changes in the OLR and 200 hPa zonal wind patterns (Fig. 4b) especially over the Pacific (Fig. 5), but also extending, to a lesser degree, into the Atlantic and Indian basins. Positive OLR anomalies (reduced convection) exceed 50 W m^{-2} in the tropical SPCZ region (120°E–180°W); with an axis of positive

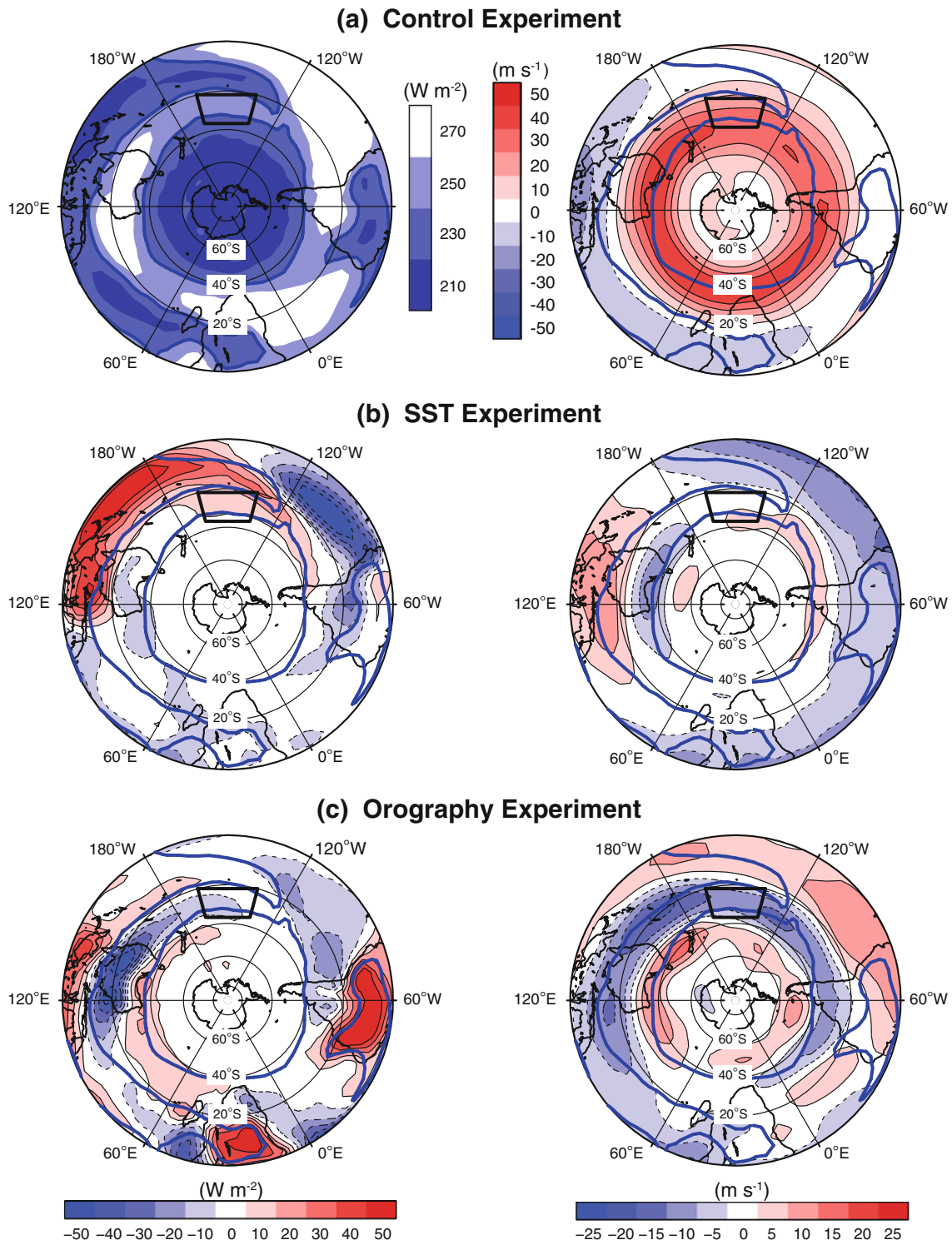


Fig. 4 DJF climatology (24 seasons) of simulated OLR (W m^{-2}) and 200 hPa zonal wind (m s^{-1}), *left and right columns* respectively; for **a** Control, **b** SST, and **c** Orography experiments. Departures from the Control simulation are shown for the SST and Orography

experiments. *Trapezoids* correspond to the OLR averaging box *A* in Fig. 3. The 240 W m^{-2} OLR contour from the Control experiment is outlined by *blue lines* in each panel

OLR anomalies oriented diagonally and coinciding with the location of the SPCZ in the Control run. To the northeast of the Control SPCZ, large OLR reductions occur

suggesting a migration of the SPCZ to the northeast. Clearly, the zonal SST gradients are related to the location and orientation of the SPCZ.

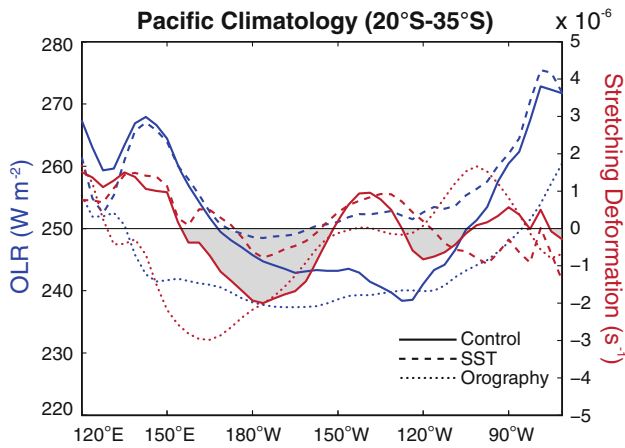


Fig. 5 DJF climatology (24 seasons) of simulated OLR (blue) and 200 hPa zonal stretching deformation (red) for the Control (solid), SST (dashed), and Orography (dotted) experiments. Averaging is done over a 15° latitude band (20°S–35°S). Gray shading depicts regions of negative zonal stretching deformation from the Control experiment

The 200 hPa zonal wind and OLR fields in the SST experiment are similar to patterns observed during El Niño events (e.g., Stretten and Zillman 1984; Trenberth 1997; Karoly and Vincent 1999). Upper tropospheric easterly winds over the West Pacific warm pool become weaker, or even westerly, while easterly wind anomalies are found throughout the remainder of the tropics. All of these features are consistent with a weaker Pacific Walker circulation. To the south, the jet stream weakens over Australia (-20 m s^{-1}) and strengthens over the eastern Pacific ($+10 \text{ m s}^{-1}$). In the subtropical region of the SPCZ, zonal stretching deformation becomes more positive, compared to the Control, and positive OLR anomalies ($10\text{--}20 \text{ W m}^{-2}$) are also observed (Fig. 5, dashed lines).

Removal of continents in the Orography experiment (Fig. 4c) does not force large convective changes in the SPCZ subtropical region, although strong OLR anomalies are observed near the location of each “continent”. The changes in the OLR distribution over Australia and Indonesia are consistent with a southward shift of the simulated tropical SPCZ, and therefore a more zonally oriented band of convection extending into the central Pacific. The replacement of Australia with a warm ocean boundary essentially enlarges the West Pacific warm pool and shifts convection poleward. Pronounced OLR and $\partial\bar{U}/\partial x$ anomalies are mostly constrained to regions outside the $180^\circ\text{W}\text{--}120^\circ\text{W}$ region, or away from the Control SPCZ (Fig. 5, dotted lines). While there are changes in the central Pacific circulation occurring with the removal of orography, negative zonal stretching deformation still occurs in the vicinity of the subtropical SPCZ and convection in this zone remains mostly unchanged.

In summary, results of the numerical experiments point to the importance of the Pacific zonal SST gradient in determining where regions of negative zonal stretching deformation exist and, hence, where OLR minima are likely to occur. The distribution of orography, both in the Northern and Southern Hemispheres, has a much smaller impact on the location of convection, at least in the central Pacific basin.

4.2 Interannual variability of the SPCZ

The numerical experiments have shown that the SST distribution dictates, to a large degree, the background quasi-stationary flow of the Southern Hemisphere; clarifying the much simpler arguments of Webster (1972) and Gill (1980). Furthermore, these patterns have attendant regions of negative zonal stretching deformation that force higher frequency disturbances to become more energetic. Slow modulations of the background SST, such as occurring during ENSO events, should modify the basic state and carry with these modifications signatures of zonal stretching deformation consistent with changes in the location of the SPCZ.

During El Niño periods, the SPCZ exhibits a distinct shift to the northeast (Stretten and Zillman 1984; Trenberth 1997; Karoly and Vincent 1999; Juillet-Leclerc et al. 2006; Vincent et al. 2009). An opposite shift towards the southwest accompanies La Niña. Similar migrations of convective and zonal wind anomalies are simulated by the AGCM SST experiment (Fig. 4b). The relationship between SST and wind distributions can be tested by seeing if the zonal SST gradient is correlated with 200 hPa zonal stretching deformation and whether changes in the zonal wind fields are matched by variations in the strength of SPCZ convection.

An SST gradient index (the difference in SST between boxes B and C shown in Fig. 3c) is developed to quantify interannual changes across the South Pacific basin. The index is standardized by removing the mean and dividing by the standard deviation. Figure 6a shows a time series of the index. Pronounced interannual variability is observed with smaller values being associated with El Niño and larger values with La Niña. For example, the gradient increase between 1998, a strong El Niño period, and 1999, a strong La Niña period, exceeds two standard deviations. Interannual variability of the off-equatorial zonal SST gradient is highly correlated with large heating anomalies in the equatorial Pacific, linked to global teleconnection processes (e.g., Trenberth 1997) and SPCZ variability. Overlaid on Fig. 6a is the linear trend suggesting that the South Pacific zonal SST gradient may have increased from 1982 to 2008. Caution should be applied when interpreting whether the long-term gradient change is significant, as

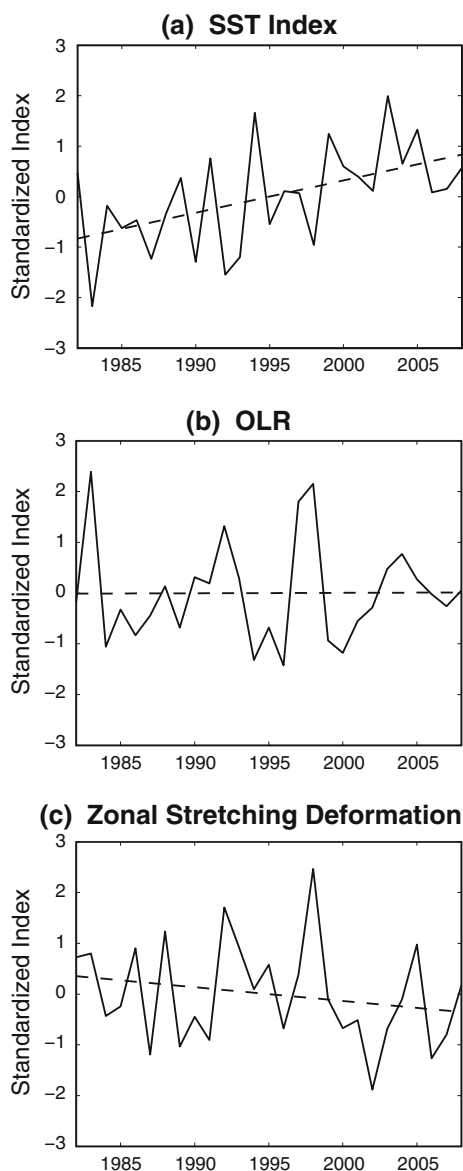


Fig. 6 Standardized SST index (a), OLR (b), 200 hPa zonal stretching deformation (c), and corresponding linear trends (dashed lines) for the averaging regions described in Fig. 3 (SST index: difference between boxes B and C; OLR and zonal stretching deformation averages: box A)

some of the 27 year signal could be attributed to interannual variability.

Figure 6b and c show the corresponding seasonal averages of OLR and 200 hPa $\partial\bar{U}/\partial x$, respectively, for box A (Fig. 3c) located in the subtropical SPCZ. The OLR and $\partial\bar{U}/\partial x$ indices are standardized using the methods discussed above to allow comparison with the SST gradient index. Interannual variability is also evident for both OLR and $\partial\bar{U}/\partial x$, with the indices typically increasing (decreasing) during El Niño (La Niña) events. These variations are out-of-phase with the SST index. Seasons experiencing an above average SST gradient typically

exhibit stronger convection (lower OLR) and stronger zonal stretching deformation near the diagonal SPCZ. During El Niño periods (reduced SST gradient), OLR is higher and $\partial\bar{U}/\partial x$ is more positive. Interestingly, the OLR index appears to show no long-term linear trend, although $\partial\bar{U}/\partial x$ does become increasingly negative as the SST gradient increases. The correlation between seasonally averaged SST gradients and 200 hPa $\partial\bar{U}/\partial x$ is -0.33 . The SST correlation with OLR is also negative and slightly larger ($r = -0.43$). A statistically significant positive correlation at the 95% level (assuming 27 independent DJF averages for the period 1982–2008) between seasonally averaged OLR and 200 hPa $\partial\bar{U}/\partial x$ ($r = 0.52$) was found, suggesting a significant decrease in OLR (i.e., stronger subtropical SPCZ) when $\partial\bar{U}/\partial x$ becomes more negative. In summary, the coherent interannual changes in the SST, the resultant changes in the background circulation, and the consequent migration of the SPCZ offer support for the hypothesis.

4.3 Synoptic and composite analyses

The period 1 December 2005–28 February 2006, representative of typical ENSO-neutral conditions, is chosen for a case study. Figure 7a shows a longitude-time plot of OLR and negative zonal stretching deformation at 200 hPa averaged between 20°S and 35°S around the entire Southern Hemisphere. Neither the OLR nor $\partial\bar{U}/\partial x$ fields have been filtered.

A striking feature of the longitude-time section is that the shaded OLR regions ($<240 \text{ W m}^{-2}$) occur in three longitudinal bands, each corresponding to a major quasi-stationary Southern Hemisphere convergence zone (SICZ 25°E–50°E, SPCZ 165°W–135°W, and SACZ 60°W–30°W) as described by Stretten (1973) and Kodama (1993). Low OLR is also occasionally observed in a narrow band near 135°E; however, moisture support does not often exist for deep convection over central Australia. A clear demarcation between the central and eastern South Pacific is apparent around 120°W in both the OLR and $\partial\bar{U}/\partial x$ distribution. The longitude-time section suggests that the SPCZ eastern border corresponds spatially and temporally to the sign change of zonal stretching deformation (Fig. 7b). Within the $\partial\bar{U}/\partial x < 0$ contours, zonal propagation speed slows down. Outside of negative stretching deformation zones, which often correspond to jet stream exit regions, any disturbance that develops is observed to propagate more rapidly eastward with a reduction in amplitude as suggested by (1, 2, 3, 4). We will quantify these observations subsequently.

Figure 7a is representative of other years as well. Figure 7b shows a comparison of the 2005–2006 DJF of OLR and 200 hPa $\partial\bar{U}/\partial x$ (dashed lines) with the 27-year

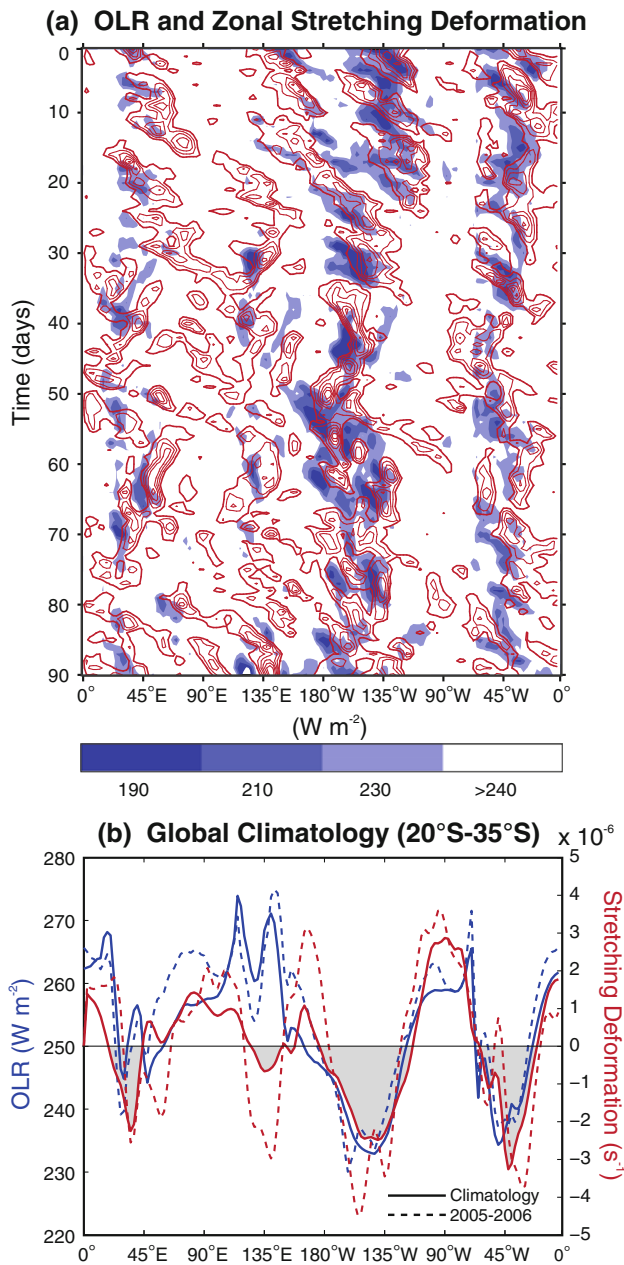


Fig. 7 **a** Hovmöller (longitude-time) of OLR (*shading* depicts values less than 240 W m^{-2}) and 200 hPa zonal stretching deformation (s^{-1} , *contours*) during 1 December 2005–28 February 2006. Zonal stretching deformation contour interval: $-4 \times 10^{-6} \text{ s}^{-1}$; starting at $-2 \times 10^{-6} \text{ s}^{-1}$ contour. Averaging is done over a 15° latitude band (20°S – 35°S). **b** 2005–2006 DJF (*dashed lines*) and 27 season climatology (*solid lines*) of OLR (*blue*) and zonal stretching deformation (*red*). *Gray shading* depicts regions of negative zonal stretching deformation, according to climatology

climatology (solid lines) of the same quantities in the same latitude band. Gray shading represents long-term average negative zonal stretching deformation. Except for subtle differences, the mean fields reflect the characteristics of the 2005–2006 case study. As with the case study, three

pronounced areas where $\partial\bar{U}/\partial x < 0$ coincides with OLR minima are apparent, each corresponding to a major Southern Hemisphere Convergence Zone plus a fourth weaker region of $\partial\bar{U}/\partial x < 0$ near 135°E . On the other hand, Fig. 7b indicates that regions where $\partial\bar{U}/\partial x > 0$ almost always have OLR values representative of shallow convection, or no convection at all.

Figure 8 presents a comparison of disturbances which pass through the eastern boundary of mean deep convection in the diagonal SPCZ (30°S , 135°W) with wave characteristics in the adjacent Southeast Indian (30°S , 105°E) and Southeast Pacific (30°S , 90°W) basins. The latter two regions are characterized by minimal convection and positive zonal stretching deformation according to climatology (Fig. 7b). OLR time series from each basin are passed through a 3–6 day Lanczos filter with 241 weights (Duchon 1979) and then scaled by the standard deviation of the respective time series to compute OLR and $\partial\bar{U}/\partial x$ linear regressions. These regressions track synoptic-scale Rossby waves more clearly than the longitude-time diagram of unfiltered data (Fig. 7a). Table 1 provides a comparison of wavelength (km), phase speed (m s^{-1}), and period (days) of synoptic wave characteristics derived from OLR regression anomalies in the SPCZ with those over the adjacent Southeast Indian and Southeast Pacific basins. Each regression depicts a period of 4–5 days, as expected when applying a synoptic (3–6 day) filtering method to subtropical OLR time series. Different phase speeds and spatial scales are observed with disturbances near the SPCZ being noticeably slower, and having shorter wavelengths, than those over neighboring basins. From Fig. 8a, “fast” waves are observed over the Southeast Indian Ocean with phase speeds of about 10.8 m s^{-1} and wavelengths of about 4,000 km. Regressions from the SPCZ base point depict “slow” waves with phase speeds and wavelengths of about 7.8 m s^{-1} and 3,000 km, respectively. OLR anomalies do not propagate east of 120°W often; however, regressions over the Southeast Pacific show sporadic convective anomalies with “fast” phase speeds (10.0 m s^{-1}) and “long” wavelengths (3,700 km) similar to those over the Southeast Indian Ocean. Results suggest that eastward phase speeds are typically divided between “fast regimes” in regions absent of deep convection (i.e., $\text{OLR} > 240 \text{ W m}^{-2}$) and “slow regimes” in convective areas shaded in Fig. 7a. Slowly propagating disturbances also have shorter wavelengths, while the periods of variability are similar in each region. This is not surprising as the frequency of the waves is conserved (Sect. 3).

Composite analyses, following the methodology of Serra et al. (2008), are constructed in order to examine more closely changes in the scale and propagation characteristics of waves moving into the diagonal SPCZ region. The regressions use the same 27 DJF seasons of daily data

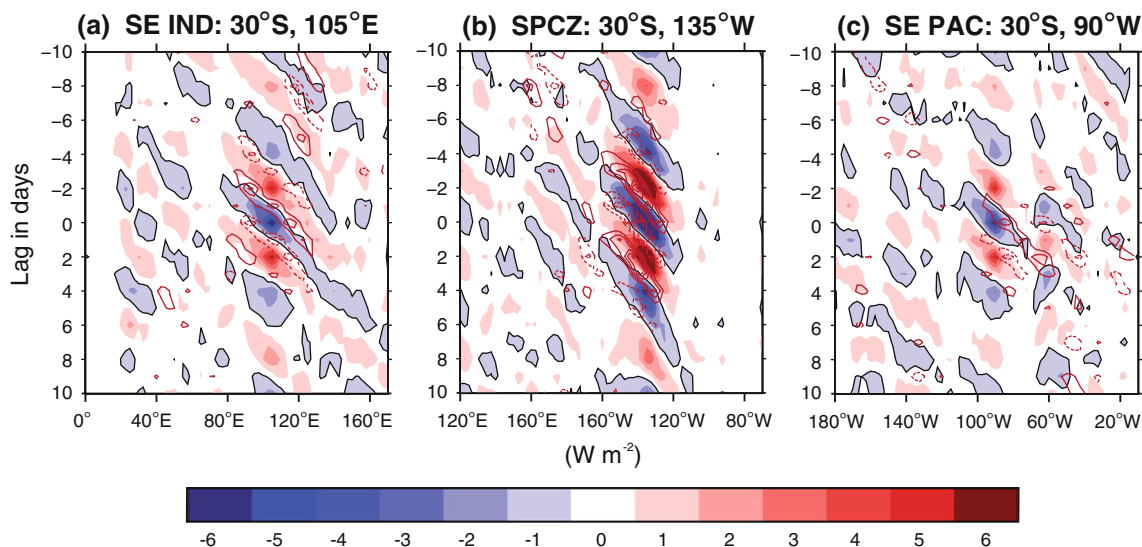


Fig. 8 a Hovmoller (longitude-lag) of OLR (W m^{-2} , shading, -1 W m^{-2} contour outlined) and 200 hPa zonal stretching deformation (s^{-1} , contours) regressions at 30°S for a 3–6 day filtered OLR base point at $30^\circ\text{S}, 105^\circ\text{E}$ (Southeast Indian basin). Zonal stretching

deformation contour interval: $2 \times 10^{-7} \text{ s}^{-1}$; starting at $\pm 4 \times 10^{-7} \text{ s}^{-1}$. Solid (dashed) lines depict negative (positive) anomalies. b and c Same as a but for base points at $30^\circ\text{S}, 135^\circ\text{W}$ (SPCZ) and $30^\circ\text{S}, 90^\circ\text{W}$ (Southeast Pacific basin), respectively

Table 1 Synoptic-wave characteristics for Southeast Indian ($30^\circ\text{S}, 105^\circ\text{E}$), SPCZ ($30^\circ\text{S}, 135^\circ\text{W}$), and Southeast Pacific ($30^\circ\text{S}, 90^\circ\text{W}$) 3–6 day filtered OLR base points

Base point	Phase speed (m s^{-1})	Wavelength (km)	Period (days)
$30^\circ\text{S}, 105^\circ\text{E}$	10.8	4,000	4.3
$30^\circ\text{S}, 135^\circ\text{W}$	7.8	3,000	4.4
$30^\circ\text{S}, 90^\circ\text{W}$	10.0	3,700	4.3

Characteristics are derived from OLR regression anomalies in Fig. 8

as used to construct the climatology of Figs. 2 and 3. Figure 9a shows a regression of unfiltered OLR (shading) and $\partial\bar{U}/\partial x$ (contours) between 120°E and 70°W based on a -20 W m^{-2} anomaly in 3–6 day filtered OLR at $30^\circ\text{S}, 135^\circ\text{W}$ for lags -10 to 10 days. Here, the longitude-lag regression is again performed for a base point at 30°S to optimize observations of OLR anomalies which propagate into the diagonal SPCZ region. Figure 9b–d shows longitude-latitude maps of the OLR and $\partial\bar{U}/\partial x$ regression for lags $-2, 0,$ and 2 days.

The 135°W regressions (Fig. 9a) show convective anomalies every 3–5 days, confirming that the Lanczos filtering method retains the correct time scale of synoptic modes of variability in the SPCZ. Set in a background climatological negative zonal stretching deformation region (Fig. 7b), $\partial\bar{U}/\partial x < 0$ anomalies (solid contours) are observed to lead most of the OLR negative anomalies by about 1 day, or 5° of longitude. Trenberth (1991), in an analysis of Southern Hemisphere storm track activity, notes similar zonal wind anomalies around 30°S and ahead of vertical motion perturbations. By tracking the negative

OLR signal westward from the base point (lag 0 days), anomalies exceeding -1 W m^{-2} (black contours) are observed to 170°W (lag -5 days). The same anomalous OLR continues eastward from the base point for about another 5 days, although only reaching 120°W . The composite disturbance propagates 35° of longitude during the first 5 days, then slows and amplifies around 135°W , and finally dissipates near the eastern SPCZ boundary.

Phase speeds become increasingly slower as disturbances propagate eastward through the SPCZ, perhaps responding to the background location of negative zonal stretching deformation. Table 2 provides a comparison of wave characteristics (indicated by $\partial\bar{U}/\partial x$ anomalies in Fig. 9b–d) at different lags within the SPCZ. At lag 0 days, wavelength and phase speed are comparable to those derived from OLR anomalies in Fig. 8b (Table 1). Table 2 confirms that wave characteristics change as disturbances propagate through the SPCZ. Wavelength shrinks from about 5,800 to 1,300 km, while the phase speed decreases from 15.2 to 3.5 m s^{-1} , between lags -2 and 2 days.

Assuming that propagation of OLR minima is representative of the group velocity (C_{gd}), (3) can be used to predict a slowdown of C_{gd} where there is negative stretching deformation of the zonal flow. Observations presented in Fig. 7b confirm that longitude bands of slow wave propagation (i.e., low OLR) are correlated spatially ($r = 0.57$) with the climatological locations of $\partial\bar{U}/\partial x < 0$. Equation (2) shows that wave energy density (ξ) can grow exponentially in regions where $\partial\bar{U}/\partial x < 0$. In fact, the magnitude of OLR anomalies show a tendency to become more enhanced as C_{gd} slows. Regression anomalies

Table 2 Synoptic-wave characteristics for a disturbance propagating through the SPCZ at Lags -2 , 0 , and 2 days

Base point	Phase speed (m s^{-1})	Wavelength (km)	Period (days)
Lag = -2 days	15.2	5,800	4.4
Lag = 0 days	7.0	2,700	4.4
Lag = 2 days	3.5	1,300	4.4

Characteristics are derived from $\partial\bar{U}/\partial x$ regression anomalies (Fig. 9b–c) using the period of OLR variability at 30°S , 135°W (Table 1)

exceeding -6 W m^{-2} are more common with the slower, and shorter, synoptic disturbances in the subtropical SPCZ compared to over the Southeast Indian or Pacific regions (Fig. 8; Table 1).

4.4 Vertical structure of modes propagating into $\partial\bar{U}/\partial x < 0$ zones

We compute \mathbf{Q} vectors in order to examine synoptic wave evolution in regions of negative zonal stretching

deformation. Following Holton (2004), we can write the quasi-geostrophic omega equation:

$$\sigma\nabla^2\omega + f_0^2\frac{\partial^2\omega}{\partial p^2} = -2\nabla\cdot\mathbf{Q} + f_0\beta\frac{\partial v_g}{\partial p} - \frac{\kappa}{p}\nabla^2J \quad (5)$$

where

$$\mathbf{Q} \equiv (Q_1, Q_2) = \left(-\frac{R}{p}\frac{\partial V_g}{\partial x}\cdot\nabla T, -\frac{R}{p}\frac{\partial V_g}{\partial y}\cdot\nabla T \right) \quad (6)$$

The equation is simplified by setting the diabatic heating term, J , equal to zero for adiabatic motions and noting that the second term on the right-hand side, related to the β effect, is small for synoptic-scale motions. As $\nabla^2\omega$ goes as $-\omega$, then (5) states that the vertical velocity field is given by the divergence of \mathbf{Q} . Specifically, rising motion occurs where \mathbf{Q} vectors are convergent ($\nabla\cdot\mathbf{Q} < 0$). Holton (2004) notes that “because such rising motion must imply vorticity stretching in the column below, cyclonic vorticity will tend to increase below a region of upper level convergent \mathbf{Q} vectors”. Thus, a test of our hypothesis is to determine whether there is an increase in the convergence of \mathbf{Q} (increase in vertical velocity and vortex tube

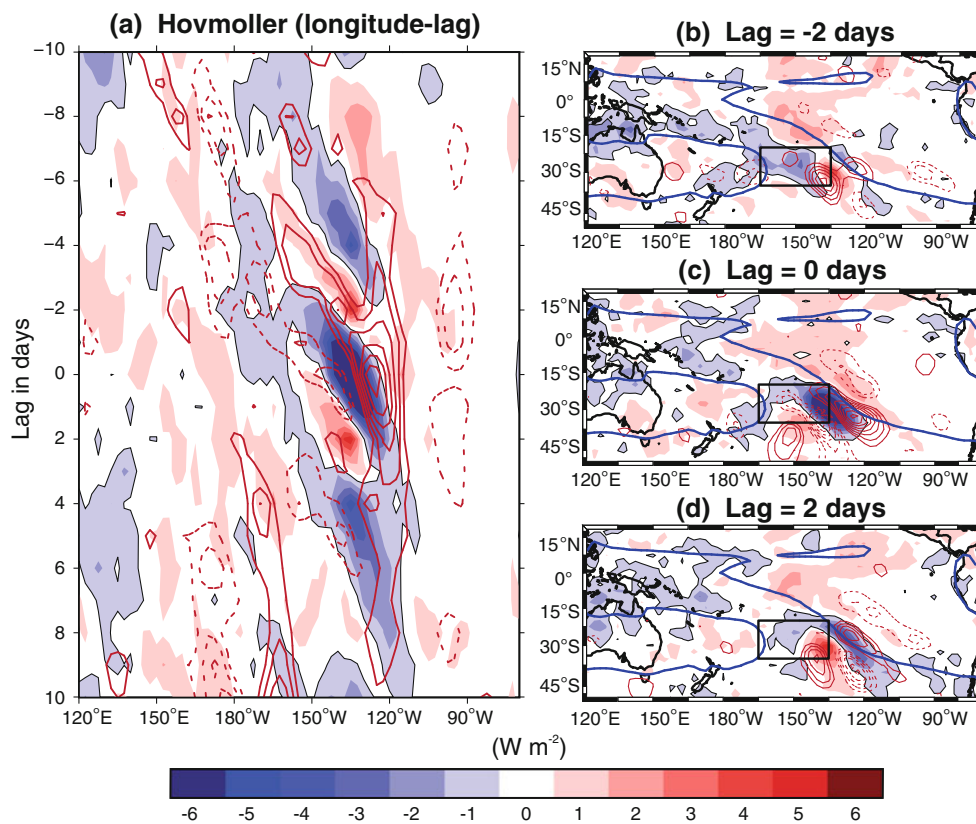


Fig. 9 a Hovmöller (longitude-lag) of OLR (W m^{-2} , shading, -1 W m^{-2} contour outlined) and 200 hPa zonal stretching deformation (s^{-1} , contours) regressions at 30°S for a 3–6 day filtered base point (-20 W m^{-2} threshold) at 30°S , 135°W . Zonal stretching deformation contour interval: $2 \times 10^{-7} \text{ s}^{-1}$; starting at $\pm 4 \times 10^{-7} \text{ s}^{-1}$.

Solid (dashed) lines depict negative (positive) anomalies. b, c, and d Same as a but for longitude-latitude regressions at Lags -2 , 0 , and 2 days, respectively. 240 W m^{-2} OLR contour (DJF climatology) outlined by blue lines

stretching) coupled with an increase of convection (measured by decreasing OLR) as a wave moves into a negative zonal stretching deformation region.

The unfiltered \mathbf{Q} vector divergence and vertical pressure velocity ($-\omega$) are regressed onto the 3–6 day filtered OLR base point described in Fig. 9. \mathbf{Q} vectors are calculated from (6) using geostrophic winds, derived from geopotential height fields, and atmospheric temperature for the 27 DJF seasons using NCEP-NCAR reanalysis data between 1,000 and 100 hPa. Daily unfiltered anomalies are averaged over a 5° latitude band which is oriented diagonally and centered along a line extending from 50°S , 155°W to 10°S , 115°W that passes through the base point located at the eastern boundary of the SPCZ (30°S , 135°W). The diagonal cross section corresponds to the maximum OLR regression anomalies, or Rossby wave propagation, observed in Fig. 9b–d. \mathbf{Q} vector regression anomalies (shading) are displayed in space-log pressure coordinates for lags of -2 , -1 , 0 , 1 , and 2 days (Fig. 10a–e, respectively). Solid (dashed) lines depict rising (sinking) velocity anomalies, with prominent regions of rising motion labeled “I”, “II”, or “III”. Figure 10f shows the location of the averaging region in relation to the SPCZ.

Each lag period in Fig. 10 shows a clear pattern of alternating positive and negative $\nabla \cdot \mathbf{Q}$ anomalies. The $\nabla \cdot \mathbf{Q}$ pattern above 200 hPa is out of phase with the anomalies below, which is evidence of convergence–divergence coupling centered along the tropopause, as is often observed with mid-latitude disturbances (e.g., Hoskins et al. 1978). Focusing on the troposphere, maximum $\nabla \cdot \mathbf{Q}$ anomalies are typically found between 300 and 400 hPa, while vertical motions are strongest around 500 hPa. Strong subsidence is observed in the eastern SPCZ (30°S , 135°W) 2 days before maximum convection reaches the base point (Fig. 10a). Rising motion (disturbance II) is centered near 40°S , 145°W and corresponds to minimum OLR observed in Fig. 9b southwest of the base point at this time. Weaker rising motion (I) is also observed northeast of the SPCZ and is perhaps associated with the previous synoptic disturbance to track through the base point. Figure 10c shows clearly that the strong rising motion associated with disturbance II has reached the SPCZ base point when maximum convection occurs at lag 0 days. Subsidence exists on both sides of the convection. Evidence of weak rising motion ($\nabla \cdot \mathbf{Q} < 0$) associated with I is still observed over the tropical central Pacific. We also begin to see the next disturbance (III) enter the region near 50°S . During the next 2 days (Fig. 10d, e), II propagates northeast and weakens while the vertical circulation associated with III amplifies, expands vertically, and approaches the SPCZ from the southwest.

Regressions of $\nabla \cdot \mathbf{Q}$ and $-\omega$ anomalies onto the filtered OLR time series provide evidence that vertical circulations, extending from the surface to the upper troposphere, are correlated with convective anomalies in the SPCZ. From the quasi-geostrophic omega Eq. (5), we note that vertical ascent is forced by \mathbf{Q} vector convergence. Mid-latitude synoptic wave propagation was shown previously (Figs. 8, 9) to slow and become more energetic in the upper tropospheric region of $\partial\bar{U}/\partial x < 0$ observed in the diagonal SPCZ. Figure 10 shows that vertical motions intensify as mid-latitude disturbances propagate into the SPCZ, slow, and increase wave energy density according to (2). Pronounced weakening of the vertical circulation (e.g., II at lag 2 days) occurs subsequently once a disturbance tracks east of the SPCZ and speeds up in the climatological region of positive zonal stretching deformation over the Southeast Pacific.

5 Conclusion and discussion

Significant correlation between cloud band orientation and large-scale circulation regions favorable for wave energy accumulation suggest a new mechanism for explaining why convection veers sharply away from the equator in the South Pacific. Specifically, there are certain regions of the atmosphere where synoptic disturbances develop and other regions where they tend to slow in their eastward propagation which promotes a region of increased wave energy density in accord with simple theoretical rules. These regions are referred to as “graveyards” by Trenberth (1976) who noted that the SPCZ was a place where synoptic disturbances tended to agglomerate and also that, on the eastern side of the SPCZ, the synoptic waves tend to be weaker. To continue the analogy, the $\partial\bar{U}/\partial x = 0$ contour demarks the boundary of Trenberth’s graveyard, while regions where $\partial\bar{U}/\partial x < 0$ denote the graveyard itself. Within this construct, we provide evidence of the three main ingredients that define the location and orientation of the SPCZ:

- (i) Baroclinic instability, associated with regional maxima of the subtropical jet stream, provides a genesis region for mid-latitude disturbances that propagate northeastward from south of Australia towards the central Pacific.
- (ii) Eastward propagation of the synoptic disturbances slows in regions of negative zonal stretching deformation while, at the same time, regional wave energy density increases and vertical circulations amplify. Such regions occur in each of the three ocean basins of the Southern Hemisphere but in particular, west of the South Pacific high.

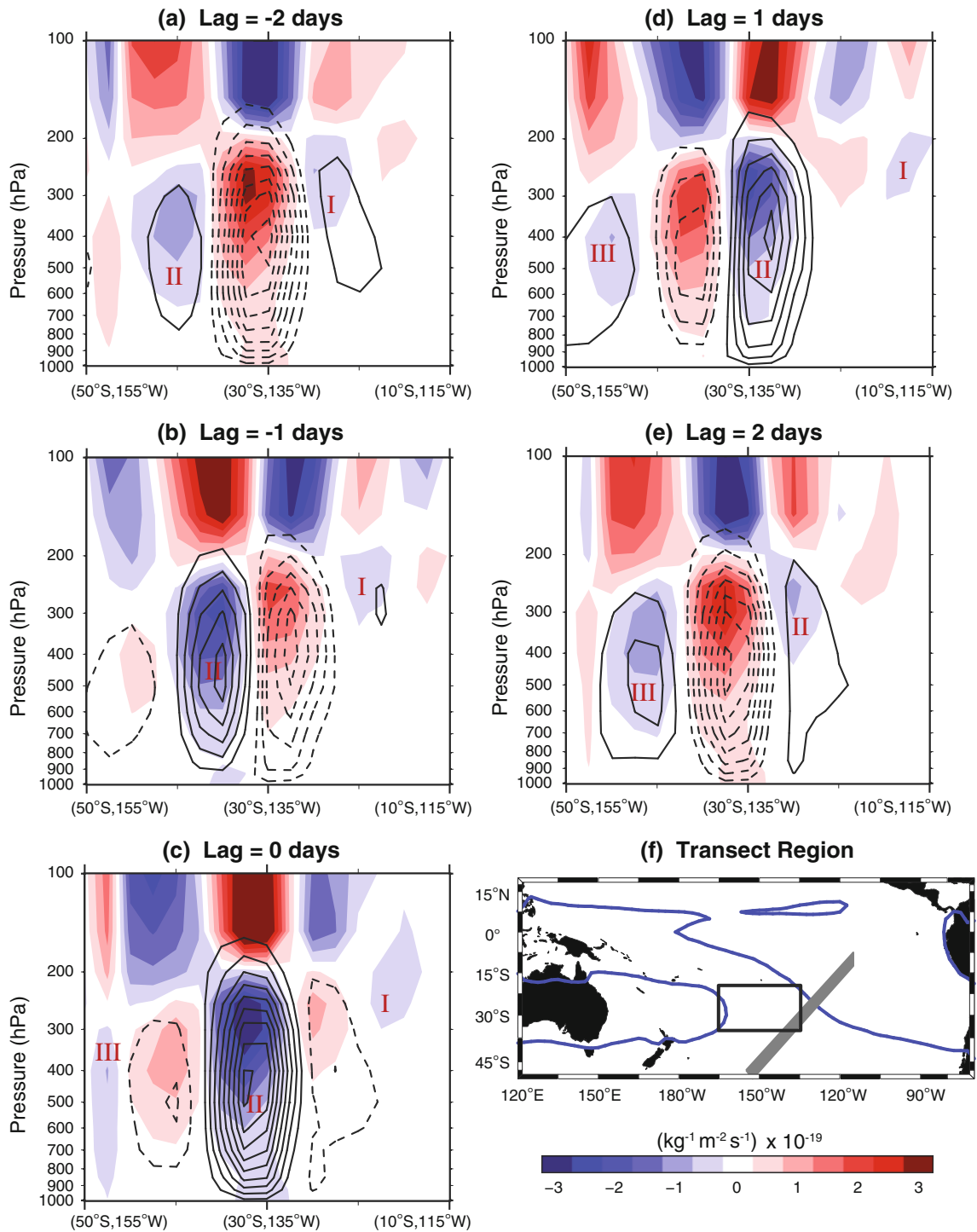


Fig. 10 Vertical regression fields of Q vector divergence ($\text{kg}^{-1} \text{m}^{-2} \text{s}^{-1}$, shading) and vertical pressure velocity ($-\omega$ contour interval: $2 \times 10^{-3} \text{ Pa s}^{-1}$; starting at $\pm 2 \times 10^{-3} \text{ Pa s}^{-1}$) averaged over a 5° latitude band centered along a line from $50^\circ\text{S}, 155^\circ\text{W}$ to $10^\circ\text{S}, 115^\circ\text{W}$ which passes through the base point used in Fig. 9. Solid (dashed)

lines depict rising (sinking) velocity anomalies. Regions of rising motion discussed in the text are labeled “I”, “II”, or “III”. **a, b, c, d,** and **e** Regressions at Lags $-2, -1, 0, 1,$ and 2 days, respectively. **f** Map of the averaging region (gray shading) and 240 W m^{-2} OLR contour (DJF climatology) outlined by blue lines

(iii) And, to the east of the negative zonal stretching deformation regions, synoptic waves accelerate eastward in a weakened state.

These three processes provide a framework for understanding where the mid-latitude disturbances originate and why the SPCZ typically exhibits a pronounced eastern

boundary of deep convection. Additionally, the SPCZ diagonal orientation is forced by the Pacific zonal SST gradient which governs the location of $\partial\bar{U}/\partial x < 0$ and, hence, the accumulation of wave energy over the central South Pacific. Conclusions were developed using satellite observations, reanalysis data, results from numerical experimentation, and simple theory. The kinematic behavior of waves in a longitudinally varying basic flow was based on two constructs: the simple theoretical development of Webster and Chang (1997) and the behavior of \mathbf{Q} vectors to study wave structure changes as disturbances propagate into regions of negative zonal stretching deformation.

Correlations on interannual timescales between the basin-scale zonal SST gradient, zonal stretching deformation, and OLR suggest that the interaction between ENSO and the SPCZ is governed to a large degree by how underlying SST anomalies force changes in the background basic state and, therefore, modify accumulation regions of mid-latitude synoptic disturbances. The location and intensity of negative zonal stretching deformation becomes more conducive for a diagonally oriented SPCZ when the SST gradient increases between the West Pacific warm pool and cooler Southeast Pacific, such as during La Niña events. Results from the AGCM sensitivity experiments support the hypothesis further that the Pacific zonal SST gradient forces convergence of the background zonal flow near the SPCZ; a necessary criterion for sustaining a diagonally oriented convective band. The $\partial\bar{U}/\partial x$ and convection relationship presents an interesting new route towards explaining how ENSO influences the South Pacific climate and, perhaps, an avenue for improved long-range forecasting. Questions concerning the feedback mechanisms of the SPCZ onto the underlying SST pattern and planetary wave structure remain as future challenges.

Finally, the contribution presented in this paper relating to why the SPCZ is oriented diagonally away from the equator may facilitate the CLIVAR/SPICE goal to develop a long-term South Pacific monitoring system capable of delivering data necessary to improve the initialization and calibration of climate forecasts.

Acknowledgments This work was made possible by support from the Climate Dynamics division of the National Science Foundation under NSF Grant ATM-0531771. We are indebted to many conversations and suggestions by Dr. H.-R. Chang and Professor D. G. Vincent. The authors thank two anonymous reviewers for useful comments.

References

- Bjerknes J, Allison LJ, Kreins ER et al (1969) Satellite mapping of Pacific tropical cloudiness. *Bull Am Meteorol Soc* 50:313–322
- Booth AL, Taylor VR (1969) Meso-scale archive and computer products of digitized video data from ESSA satellites. *Bull Am Meteorol Soc* 50:431–438
- Bracco B, Kucharski F, Kallummal R et al (2004) Internal variability, external forcing and climate trends in multi-decadal AGCM ensembles. *Clim Dyn* 23:659–678
- Bretherton FP, Garrett CJR (1968) Wavetrains in inhomogeneous moving media. *Proc R Soc Lond A302*:529–554
- Carvalho LMV, Jones C, Liebmann B (2002) Extreme precipitation events in southeastern South America and large-scale convective patterns in the South Atlantic Convergence Zone. *J Clim* 15:2377–2394
- Chang HR, Webster PJ (1990) Energy accumulation and emanation at low latitudes. Part II: nonlinear response to strong episodic forcing. *J Atmos Sci* 47:2624–2644
- Chang HR, Webster PJ (1995) Energy accumulation and emanation at low latitudes. Part III: forward and backward accumulation. *J Atmos Sci* 52:2384–2403
- Duane G, Webster PJ, Weiss J (1999) Co-occurrence of northern and southern hemisphere blocks as partially synchronized chaos. *J Atmos Sci* 56:4183–4205
- Duchon C (1979) Lanczos filtering in one and two dimensions. *J Appl Meteorol* 18:1016–1022
- Eastin M, Vincent D (1998) A 6-year climatology of vertical mean and shear components of kinetic energy for the Australian-South Pacific jet stream. *J Clim* 11:283–291
- Folland CK, Renwick JA, Salinger MJ (2002) Relative influences of the Interdecadal Pacific Oscillation and ENSO on the South Pacific Convergence Zone. *Geophys Res Lett* 29(13):1643. doi: [10.1029/2001GL014201](https://doi.org/10.1029/2001GL014201)
- Ganachaud A, Kessler W, Wijffels S et al (2007) Southwest Pacific Ocean circulation and climate experiment (SPICE)-Part I. Scientific background. International CLIVAR Project Office, CLIVAR Publication Series No. 111, NOAA OAR Special Report, NOAA/OAR/PMEL, Seattle, WA, p 37
- Gibson JK, Kallberg P, Uppala S et al (1997) ECMWF re-analysis. Project report series. I. ERA description. European Centre for Medium-Range Weather Forecasts, Reading, UK
- Gill AE (1980) Some simple solutions for heat-induced tropical circulation. *Q J R Meteorol Soc* 106:447–462
- Godshall FA (1968) Intertropical Convergence Zone and mean cloud amount in tropical Pacific Ocean. *Mon Weather Rev* 96:172–175
- Graham NE, Barnett TP (1987) Sea surface temperature, surface wind divergence, and convection over tropical oceans. *Science* 238:657–659
- Held IM, Suarez MJ (1994) A proposal for the intercomparison of the dynamical cores of atmospheric general circulation models. *Bull Am Meteorol Soc* 75:1825–1830
- Holton JR (2004) An introduction to dynamic meteorology, 4th edn. Elsevier Academic Press, Burlington, MA, p 535
- Hoskins BJ, Hodges KI (2005) A new perspective on Southern Hemisphere storm tracks. *J Clim* 18:4108–4129
- Hoskins BJ, Draghici I, Davies HC (1978) A new look at the ω -equation. *Q J R Meteorol Soc* 104:31–38
- Juillet-Leclerc A, Thiria S, Naveau P et al (2006) SPCZ migration and ENSO events during the 20th century as revealed by climate proxies and a Fiji coral. *Geophys Res Lett* 33:L17710. doi: [10.1029/2006GL025950](https://doi.org/10.1029/2006GL025950)
- Kalnay E, Kanamitsu M, Kistler R et al (1996) The NCEP/NCAR 40-year reanalysis project. *Bull Am Meteorol Soc* 77:437–470
- Karoly DJ, Vincent DG (1999) Meteorology of the Southern Hemisphere, 2nd edn. *Meteor Monogr* 27:101–117
- Kiladis G, Storch H, Loon H (1989) Origin of the South-Pacific Convergence Zone. *J Clim* 2:1185–1195
- Kistler R, Kalnay E, Collins W et al (2001) The NCEP–NCAR 50-year reanalysis: monthly means CD-ROM and documentation. *Bull Am Meteorol Soc* 82:247–267

- Kodama Y (1993) Large-scale common features of sub-tropical Convergence Zones. *J Meteorol Soc Jpn* 17:581–610
- Kornfield J, Hasler AF, Hanson KJ et al (1967) Photographic cloud climatology from ESSA 3 and 5 computer produced mosaics. *Bull Am Meteorol Soc* 48:878–883
- Kucharski F, Molteni F, Bracco A (2006) Decadal interactions between the western tropical Pacific and the North Atlantic Oscillation. *Clim Dyn* 26:79–91
- Kucharski F, Bracco A, Yoo JH et al (2009) A Gill-Matsuno-type mechanism explains the tropical Atlantic influence on African and Indian monsoon rainfall. *Q J R Meteorol Soc* 135:569–579
- Kuhnel I (1989) Tropical-extratropical cloudband climatology based on satellite data. *Int J Climatol* 9:441–463
- Leese JA, Novak CS, Taylor VR (1970) The determination of cloud pattern motions from geosynchronous satellite image data. National Environmental Satellite Center, Washington, DC
- Liebmann B, Smith CA (1996) Description of a complete (interpolated) outgoing longwave radiation dataset. *Bull Am Meteorol Soc* 77:1275–1277
- Lighthill J (1978) *Waves in fluids*. Cambridge University Press, London. doi:10.2277/0521010454
- Lin JL (2007) The double-ITCZ problem in IPCC AR4 coupled GCMs: ocean–atmosphere feedback analysis. *J Clim* 20:4497–4525
- Lindzen RS, Nigam S (1987) On the role of sea-surface temperature-gradients in forcing low level winds and convergence in the tropics. *J Atmos Sci* 44:2418–2436
- Lintner BR, Neelin JD (2008) Eastern margin variability of the South Pacific Convergence Zone. *Geophys Res Lett* 35:L16701. doi:10.1029/2008GL034298
- Molteni F (2003) Atmospheric simulations using a GCM with simplified physical parametrizations. I: model climatology and variability in multi-decadal experiments. *Clim Dyn* 20:175–191
- Nicholson SE (2003) Comment on “The South Indian Convergence Zone and interannual rainfall variability over Southern Africa” and the question of ENSO’s influence on Southern Africa. *J Clim* 16:555–562
- Reynolds RW, Rayner NA, Smith TM et al (2002) An improved in situ and satellite SST analysis for climate. *J Clim* 15:1609–1625
- Rickenbach TM, Ferreira RN, Halverson JB et al (2002) Modulation of convection in the southwestern Amazon basin by extratropical stationary fronts. *J Geophys Res*. doi:10.1029/2000JD000263
- Rodwell MJ, Hoskins BJ (2001) Subtropical anticyclones and summer monsoons. *J Clim* 14:3192–3211
- Rowell DP (2001) Teleconnections between the tropical Pacific and the Sahel. *Q J R Meteorol Soc* 127:1683–1706
- Serra YL, Kiladis GN, Cronin MF (2008) Horizontal and vertical structure of easterly waves in the Pacific ITCZ. *J Atmos Sci* 65:1266–1284
- Streten NA (1970) A note of the climatology of the satellite observed zone of high cloudiness in the central South Pacific. *Aust Meteorol Mag* 18:31–38
- Streten NA (1973) Some characteristics of satellite-observed bands of persistent cloudiness over the Southern Hemisphere. *Mon Weather Rev* 101:486–495
- Streten NA, Zillman JW (1984) Climate of the South Pacific Ocean. In: van Loon H (ed) *World survey of climatology*, vol 15: The Oceans. Elsevier, New York
- Takahashi K, Battisti DS (2007a) Processes controlling the mean tropical Pacific precipitation pattern. Part I: The Andes and the Eastern Pacific ITCZ. *J Clim* 17:3434–3451
- Takahashi K, Battisti DS (2007b) Processes controlling the mean tropical Pacific precipitation pattern. Part II: The SPCZ and the southeast Pacific dry zone. *J Clim* 20:5696–5706
- Taljaard JJ (1972) Synoptic meteorology of the Southern Hemisphere. In: Newton CW (ed) *Meteorology of the Southern Hemisphere*. Meteorol Monogr 13:139–211
- Todd M, Washington R (1998) Extreme daily rainfall in southern African and southwest Indian Ocean tropical-temperate links. *S Afr J Sci* 94:64–70
- Todd M, Washington R (1999) Tropical-temperate links in southern Africa and southwest Indian Ocean satellite-derived rainfall. *Int J Clim* 19:1601–1616
- Todd M, Washington R, James T (2003) Characteristics of summer-time daily rainfall variability over South America and the South Atlantic Convergence Zone. *Meteorol Atmos Phys* 83:89–108
- Toma VE, Webster PJ (2009) Oscillations of the intertropical Convergence Zone and the genesis of easterly waves. Part I: diagnostics and theory. *Clim Dyn*. doi:10.1007/s00382-009-0584
- Tomas R, Webster PJ (1994) Horizontal and vertical structure of cross-equatorial wave propagation. *J Atmos Sci* 51:1417–1429
- Torrence C, Compo GP (1998) A practical guide to wavelet analysis. *Bull Am Meteorol Soc* 79:61–78
- Trenberth KE (1976) Spatial and temporal variations of the Southern Oscillation. *Q J R Meteorol Soc* 102:639–653
- Trenberth KE (1991) Storm tracks in the Southern Hemisphere. *J Atmos Sci* 48:2159–2178
- Trenberth KE (1997) The definition of El Niño. *Bull Am Meteorol Soc* 78:2771–2777
- Trenberth KE, Stepaniak DP (2003) Seamless poleward atmospheric energy transports and implications for the Hadley circulation. *J Clim* 16:3706–3722
- Trenberth KE, Stepaniak DP, Caron JM (2000) The global monsoon as seen through the divergent atmospheric circulation. *J Clim* 13:3939–3993
- van Heerden J, Taljaard JJ (1998) Africa and the surrounding waters. In: Karoly DJ, Vincent DG (eds) *Meteorology of the Southern Hemisphere*, 2nd edn. Meteor Monogr 49:141–174
- van Loon H, Jenne RL (1972) The zonal harmonic standing waves in the Southern Hemisphere. *J Geophys Res* 77:992–1003
- Vincent DG (1994) The South Pacific Convergence Zone (SPCZ): a review. *Mon Weather Rev* 122:1949–1970
- Vincent EM, Lengaigne M, Menkes CE et al (2009) Interannual variability of the South Pacific Convergence Zone and implications for tropical cyclone genesis. *Clim Dyn*. doi:10.1007/s0038200907163
- Webster PJ (1972) Response of tropical atmosphere to local, steady forcing. *Mon Weather Rev* 100:518–541
- Webster PJ (1982) Seasonality in the local and remote atmospheric response to sea surface temperature anomalies. *J Atmos Sci* 39:29–40
- Webster PJ, Chang HR (1988) Equatorial energy accumulation and emanation regions: Impacts of a zonally varying basic state. *J Atmos Sci* 45:803–829
- Webster PJ, Chang HR (1997) Atmospheric wave propagation in heterogeneous flow: basic flow controls on tropical–extratropical interaction and equatorial wave modification. *Dyn Atmos Oceans* 27:91–134
- Webster PJ, Holton JR (1982) Cross-equatorial response to middle-latitude forcing in a zonally varying basic state. *J Atmos Sci* 39:722–733
- Yoshikane T, Kimura F (2003) Formation mechanism of the simulated SPCZ and Baiu front using a regional climate model. *J Atmos Sci* 60:2612–2632
- Zhang C, Webster PJ (1989) Effects of zonal flows on equatorially trapped waves. *J Atmos Sci* 46:3632–3652